OPEN

Translational Retinal Imaging

Jorge Orellanos-Rios, MD, Sho Yokoyama, MD†, Alauddin Bhuiyan, PhD‡, Liang Gao, PhD§, Oscar Otero-Marquez, MD¶, and R. Theodore Smith, MD, PhD¶*

Abstract: The diagnosis and treatment of medical retinal disease is now inseparable from retinal imaging in all its multimodal incarnations. The purpose of this article is to present a selection of very different retinal imaging techniques that are truly translational, in the sense that they are not only new, but can guide us to new understandings of disease processes or interventions that are not accessible by present methods. Quantitative autofluorescence imaging, now available for clinical investigation, has already fundamentally changed our understanding of the role of lipofuscin in age-related macular degeneration. Hyperspectral autofluorescence imaging is bench science poised not only to unravel the molecular basis of retinal pigment epithelium fluorescence, but also to be translated into a clinical camera for earliest detection of age-related macular degeneration. The ophthalmic endoscope for vitreous surgery is a radically new retinal imaging system that enables surgical approaches heretofore impossible while it captures subretinal images of living tissue. Remote retinal imaging coupled with deep learning artificial intelligence will transform the very fabric of future medical care.

Key Words: endoscopic surgery, hyperspectral imaging, quantitative autofluorescence, telemedicine, translational medicine

(*Asia Pac J Ophthalmol (Phila)* 2020;9:269–277)

The diagnosis and treatment of medical retinal disease is now inseparable from retinal imaging in all its multimodal incarnations. The purpose of this article is to present a selection of very different retinal imaging techniques that are truly translational, in the sense that they are not only new, but can guide us to new understandings of disease processes or interventions that are not accessible by present methods. Quantitative autofluorescence (qAF) imaging, now available for clinical investigation, has already fundamentally changed our understanding of the role of lipofuscin (LF) in age-related macular degeneration (AMD). Hyperspectral autofluorescence (AF) imaging is bench science poised not only to unravel the molecular basis of retinal pigment epithelium (RPE) fluorescence, but also to be translated into a clinical camera for earliest detection of AMD. The ophthalmic endoscope for vitreous surgery is a radically new retinal imaging system that enables surgical approaches heretofore impossible while it captures subretinal images of living tissue. Remote retinal imaging coupled with deep learning (DL) artificial intelligence will transform the very fabric of future medical care.

From the *Fundación Oftalmológica Los Andes, Vitacura, Santiago de Chile, Chile; †Department of Ophthalmology, Japan Community Healthcare Organization, Chukyo Hospital, Nagoya, Aichi, Japan; ‡iHealthScreen Inc, New York, NY, USA; §Department of Biomedical Engineering, UCLA, LA, Los Angeles, CA, USA; and ¶Department of Ophthalmology, Icahn School of Medicine at Mount Sinai, New York, NY, USA.

Submitted March 3, 2020; accepted April 3, 2020.
Financial Support: NIH R01 EY015520 (RTS).
The authors have no conflicts of interest to disclose.

Correspondence: R. Theodore Smith, Department of Ophthalmology, Icahn School of Medicine at Mount Sinai, 1 Gustave L. Levy Place, New York, NY 10029. E-mail: rts1md@gmail.com.

ISSN: 2162-0989
DOI: 10.1097/APO.0000000000000292

TRANSLATIONAL TOPIC 1. qAF IMAGING

qAF is a novel, innovative imaging modality to measure in vivo the LF-related fundus autofluorescence (FAF) from the RPE. This method, introduced in 2011 by Delori et al,[1] is performed by calibrating the FAF image to an internal reference of known fluorescence efficiency within a confocal scanning laser ophthalmoscope (cSLO). This makes it possible to reproducibly quantify and compare the FAF intensity between subjects and across the time.

qAF in AMD

qAF has provided a new understanding of the pathogenesis of age-related macular degeneration (AMD). One of the first applications of qAF technology in clinical AMD was published in 2016 by Gliem et al.[2] They studied 40 patients with AMD aged 65 years or younger. Most of the eyes had intermediate AMD. Phenotypic classification revealed 70% of patients with soft drusen, 20% with cuticular drusen, and 10% with reticular pseudodrusen (RPD). Compared with the controls, statistical analysis revealed lower qAF values in the overall AMD cohort and in all subgroups. Hence, they found no evidence for increased LF in eyes with early to intermediate stage of AMD. However, patients older than 65 years and those with advanced AMD were not included.

In 2018, Orellana-Rios et al[3] complemented the results of Gliem's group. They used qAF to measure FAF intensities only in pseudophakic eyes with 3 nonneovascular AMD phenotypes aged 65 years or older and compared them with normal age-matched controls. They also confirmed that qAF levels were also statistically significant higher in control participants than in all patients with AMD, especially in eyes with subretinal drusenoid deposits aka RPD.[4] The study showed that qAF decreased from normal aging to early to late AMD.

A subsequent analysis in eyes with geographic atrophy (GA) and reticular macular disease[5,6] or RPD evaluated qAF in the junctional zone and outside atrophic areas along with spectral-domain optical coherence tomography (SD-OCT) to correlate qAF with retinal structure. They found that areas with the highest qAF intensities, in the border zone of GA, were associated with

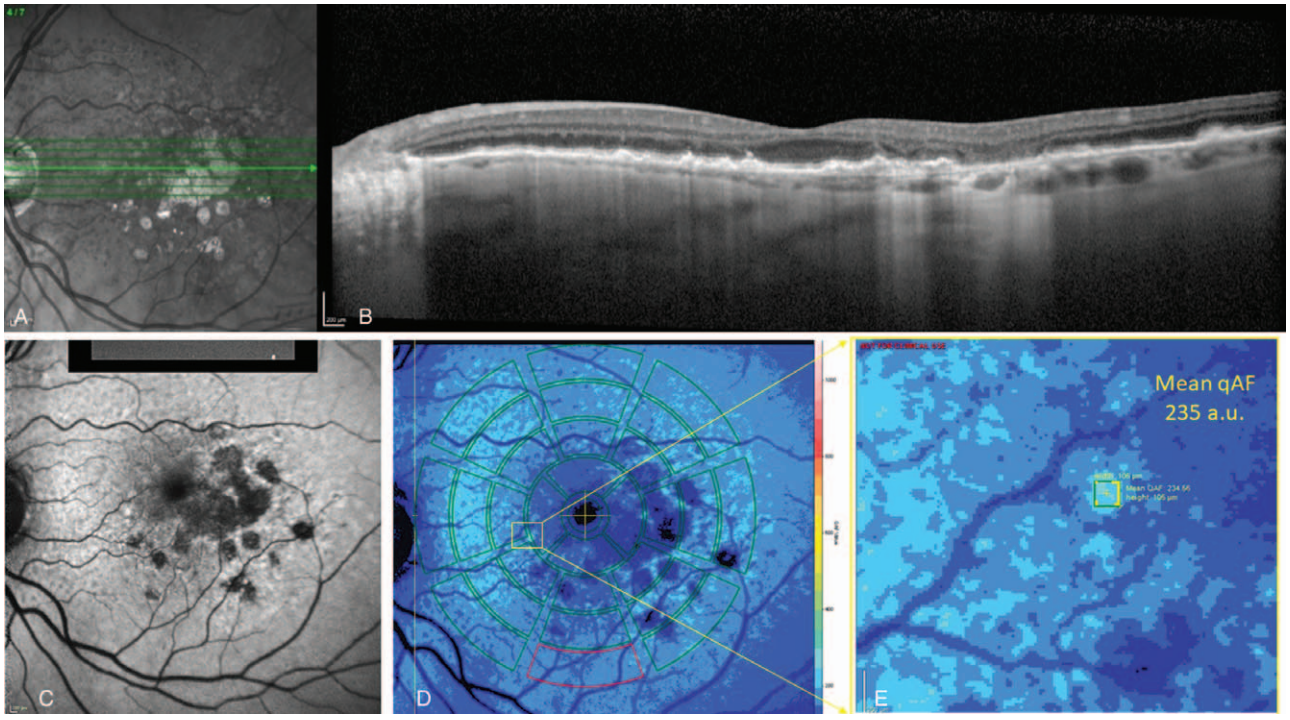

FIGURE 1. qAF in a patient with multilobular geographic atrophy (GA). A reticular macular disease (RMD) phenotype in a 78-year-old woman as seen on (A) near-infrared reflectance and (B) enhanced depth imaging optical coherence tomography (EDI-OCT) B scan. C, The qAF values were calculated by measuring the mean gray levels and the internal reference above to obtain a color-coded image with a reference bar showing qAF intensities in artificial units. Accordingly, this patient with late age-related macular degeneration can be studied by using overlay tools such as Delori pattern (D) or a region-of-interest (E), within the junctional zone of GA in RMD. qAF indicates quantitative autofluorescence.

thickening of the RPE-Bruch membrane (BrM) band on SD-OCT corresponding to hyper-FAF spots. They suggested that focal hyper-FAF intensities may represent islands of activated or stacked RPE cells seen on SD-OCT for progression in GA as previously attributed and not primarly to LF accumulation within individual cells. (Fig. 1)

In summary, as FAF has been established as a qualitative tool to visualize LF components in vivo, qAF has demonstrated quantitatively a decline in LF with decreasing RPE health and increasing severity of non-neovascular AMD. This suggests that loss of LF fluorophores, not increase, signifies AMD progression.

Since the qAF imaging tool has been highlighted as a potential indicator of progression in AMD, Reiter et al[7] prospectively studied eyes with early and intermediate AMD to examine the association between drusen volume (DV) and qAF. They found that qAF steadily decreased with age whereas DV increased in about half of patients, a quantitative corroboration that FAF and the buildup of drusen are uncoupled processes in AMD. Although DV has been described as a monitoring marker in AMD with adequate repeatability and reproducibility,[8] qAF changes might be more precise and easily monitored in long-term studies.

Lastly, Wang et al[9] presented an informative study on qAF in smokers compared with nonsmokers in healthy volunteers. Since smoking is one of the most significant modifiable factor for the development and progression of AMD, these authors hypothesized that qAF might be an appropiate modality to clinically assess its impact on RPE fluorophores due to oxidative damage causing a buildup of other fluorescent compounds. However, despite of having found higher qAF intensities in eyes with positive smoking history, these outcomes were not statistically significant.

qAF in Stargardt Disease

Stargardt disease (STGD1) is the most common form of hereditary recessive macular distrophy, with a prevalence of approximately 1:10,000.[10] Disease-related variants in the *ABCA4* gene, which encodes a protein that is required to remove byproducts from photoreceptor outer segment disc membranes, leads to accumulation of LF fluorophores in the RPE cells.[11]

Burke et al,[12] in a study of 42 patients with *ABCA4* mutations found elevated qAF levels, in some young patients up to 8-fold higher than in healthy eyes. The earlier age of STGD1-onset, the higher the levels of qAF. However, some *ABCA4* variants have shown a decrease with age or near-normal qAF levels, specifically for patients harboring the p.Gly1961Glu mutation. The highest qAF levels values were observed for eyes with numerous retinal flecks. Conversely, when flecks have resorbed and migrated centripetally from the central retina, leaving lobules of atrophy in the macula, qAF centrally decreased (Fig. 2). The important point is that qAF values change with the disease stage.

Some authors have attributed the progressive loss of qAF to photobleaching of the bisretinoid fluorophores and loss of diseased RPE cells.[13] Thus, despite a massive LF accumulation in STGD1 early in life, this is followed by a steady downward trend. Hence, a substantial fraction of STGD1 patients do not present with increased LF-mediated FAF, probably due to these processes.

qAF helps differentiate Stargardt disease from other retinal dystrophies.[14] Patients having ABCA4-associated disease can present with a variety of different phenotypes such as bull's eye maculopathy[15] or a pattern dystrophy phenotype. Higher qAF levels were found in ABCA4-positive patients, whereas qualitative features of FAF and SD-OCT images did not serve

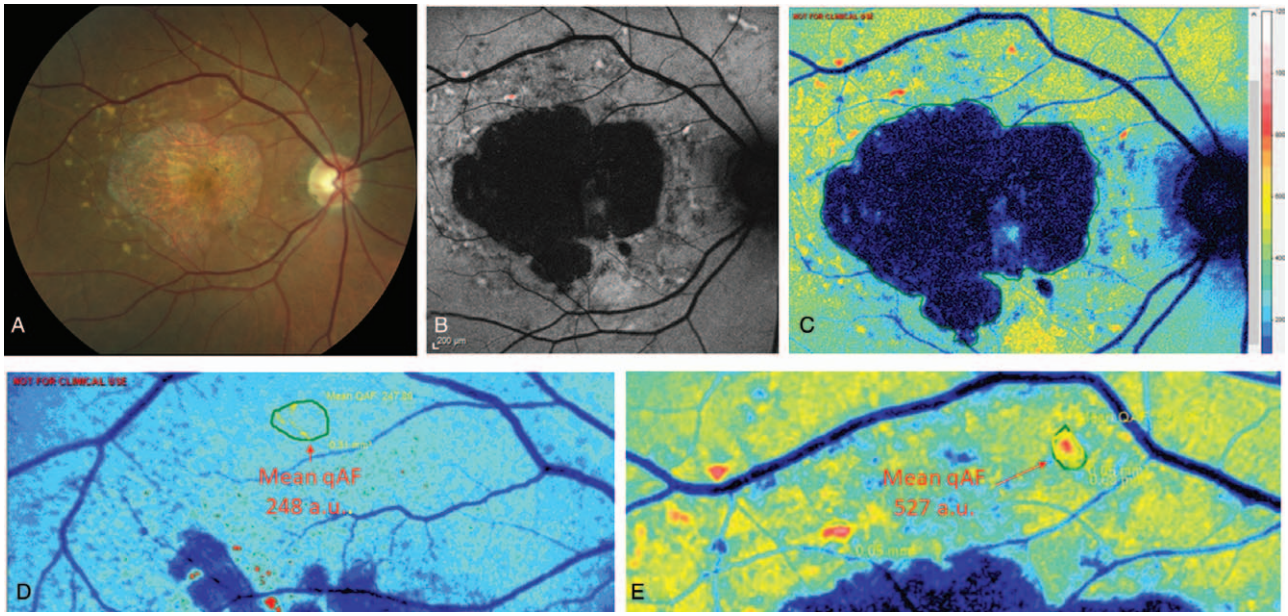

FIGURE 2. qAF in a 74-year-old man with Stargardt disease. An illustrative case of the right eye as seen on (A) color fundus photography. (B) The mean gray values were measured to obtain a color-coded qAF map (C). The highest qAF values corresponded to hyperAF pisciform retinal flecks, superior to GA. An evident difference can be noted between an age-matched patient with AMD (D) and this patient with Stargardt disease (E). A comparison of a ROI in the perilesional zone of GA in AMD and Stargardt-associated GA revealed a 2-fold higher qAF values in the latter (248 au v/s 528 au). Hence the importance of the qAF method to differentiate AMD from retinal dystrophies. (qAF imaging courtesy of Wei Wei MD). qAF indicates quantitative autofluorescence.

to distinguish them from ABCA4-negative ones. Thus, the qAF method increases the odds of finding causal mutations in genes other than *ABCA4* such as *PRPH2/RDS*-associated retinal disease,[16] by acting as a guide for genetic testing.

qAF in Retinitis Pigmentosa

qAF allows identification of a typical hyperautofluorescent ring, which defines an area of disease activity. Its inner border delimits an area, interior to the ring, that exhibits normal function.[17] Pronounced retina degeneration peripheral to the outer border of the ring is also confirmed by OCT-B scans. The ring moves inward as disease progresses coincident with damage to the photoreceptor ellipsoid zone, thinning of the outer nuclear layer, and appearance of hyperreflective intraretinal foci. qAF in these rings is about 15% higher than normal controls, perhaps due to some combination of unmasking of a still intact RPE/Bruch band from shielding by photopigment from the blue light of the SLO, or an increase in the formation of LF from phagocytosis of damaged photoreceptors.[18]

qAF in Best Vitelliform Macular Dystrophy

The qAF intensities outside the vitelliform lesion are not elevated relative to that observed in healthy eyes. However, qAF levels are elevated within the hyperreflective material that characterizes this retinal disease.[19]

qAF in Other Retinal Diseases

The value of the qAF technology as a disease biomarker for progression has been explored not only in retinal degenerations but also in pseudoxanthoma elasticum[20] (PXE), an inherited disease caused by mutations in the *ABCC6* gene.

Reduced qAF levels were obtained in eyes of patients with PXE relative to control healthy eyes, especially in nasal areas where BrM changes are considered to be the most severe. A diseased BrM may lead to RPE atrophy or impaired RPE metabolism with slowing of the visual cycle. Both may be possible explanations for reduced LF flurophores in the RPE layer as stated by Gliem's group.

PXE, a model of disease for BrM pathology, and AMD share some phenotypic similarities and reduced qAF values, indicating reduced LF levels within RPE cells, although AMD has a more complex pathophysiology with several contributing pathways to explain these findings.

The qAF imaging technique itself has intrinsic biologic limitations to its capacity for directly measuring LF concentration in the RPE. Different packing, distribution or composition of fluorophores (ie, melanin and melanolipofuscin) or extracellular blockage of the signal by extracellular structures (RPD) may affect qAF intensities. Further studies focusing on the exact composition and distribution of macular fluorophores such as the use of the promising hyperspectral imaging analysis[21,22] are needed.

Translational Significance. qAF declines with decreasing RPE health and increasing severity of non-neovascular AMD. Therefore, loss of LF fluorophores, not increase, signifies AMD progression, and rebuts old theories of LF toxicity being in part responsible for AMD. Hence, treatments for AMD that propose to reduce the LF content of the RPE, such as with visual cycle modulators, lack physiological rationale. If such treatment deprives the retina of vitamin A, then adverse effects such as night blindness might even result. Research efforts would be better directed to finding out *why* the RPE loses its fluorophores in AMD.

Translational Topic 2. Hyperspectral AF Imaging for Detection of AMD

Soft drusen and basal linear deposit are the lipid-rich material of the Oil Spill on BrM, and the fundamental hallmark of early AMD. Drusen are focal and recognizable clinically. Basal linear deposit, the histopathologic precursor of drusen, is thin, diffuse, and invisible clinically, even on high-resolution OCT, but is detectable *ex vivo* on hyperspectral AF imaging, as we will demonstrate. In this section, we will review the basic principles of AF and hyperspectral imaging, then describe hyperspectral AF imaging with specific findings relevant for AMD, and future translational imaging applications.

AF Imaging

Clinical FAF imaging is well-established in retinal practice. LF granules within the RPE emit a broad band fluorescence when stimulated by blue light. This LF-related fluorescence then is captured by a cSLO, the Heidelberg Spectralis (Heidelberg Engineering, Heidelberg, DE), and displayed as a 2D gray scale intensity image (Fig. 3). When the RPE undergoes GA in advanced AMD, the LF granules are lost and the FAF image turns dark in this area. It is generally accepted that FAF imaging is the most accurate way to detect and measure GA in AMD,[23] and RPE atrophy in other diseases like STGD.[24]

Hyperspectral Imaging

Hyperspectral imaging is a general imaging modality combining spectral (wavelength) and spatial data of light coming from the object being imaged. The object can be a tiny piece of tissue or a large portion of the Earth's surface, as in satellite imagery, and is generally considered to be 2-dimensional. Hyperspectral images are actually stacks of individual images, each image acquired in a narrow spectral band across the wavelengths of interest, for example, the visible spectrum, and a separate 2D image is acquired at each wavelength. The resulting stack of images is called a hyperspectral cube that contains 2 spatial dimensions and 1 spectral (wavelength) dimension. Because the human eye cannot visualize this complicated data, the goal is to understand the data by decomposing it with advanced mathematical tools like non-negative matrix factorization into a few main spectral signatures of a few main physical sources in the original object with their corresponding spatial localizations.[25,26] The process of resolving these spectra and finding their spatial distributions is called "hyperspectral image unmixing." For example, to monitor oxygen saturation in the retinal vessels,[27] the physical sources of interest are the molecules hemoglobin and oxy-hemoglobin Hgb and HgbO2, and their spectral signatures are their absorption spectra. Because hyperspectral imaging is noninvasive, it is an ideal method for clinical use (Fig.4).

Hyperspectral AF Imaging in AMD

We have applied these techniques to analyze the AF properties of the LF fluorophores of the RPE in health and disease, particularly AMD. Twenty-micrometer-thin flatmounts of human RPE attached to BrM (RPE/BrM) from 20 eyes with and without AMD were prepared by removing the choroid and neurosensory retina, as previously described.[28] Hyperspectral AF emission images were acquired from each tissue from 420 to 720 nm (spectral channel width: 10 nm) with a hyperspectral camera (Nuance FX; Caliper LifeSciences, Waltham, MA) attached to a wide-field epifluorescence microscope (Axio Imager A2; Carl Zeiss, Jena, Germany) with band-pass filter cubes for AF excitation (Chroma Technology Corp, Bellows Falls, VT), an external mercury arc light source (X-Cite 120Q; Lumen Dynamics Group, Inc, Mississauga, ON, Canada), and a 40X oil objective (numerical aperture = 1.4). Three hypercubes were acquired, one at each of 3 excitation wavelengths (λ_{ex} 436 nm, λ_{ex} 450 nm, and λ_{ex} 480 nm) for simultaneous solution by non-negative matrix factorization as previously described with a custom MATLAB-based programs (MATLAB, release 2013a; MathWorks, Inc., Natick, MA) to recover the abundant spectra and their corresponding tissue localizations.[26]

Our first results, with 2 excitations, λ_{ex} 436 nm and λ_{ex} 480 nm, found smooth, well-defined spectra S1-S3 and abundances consistent with LF/melanolipofuscin perinuclear localization at each location. In addition, for AMD eyes with drusen, a distinct short wavelength spectrum spectrum for drusen (SDr) was found for drusen and subRPE deposits with an emission near 510 nm (Fig. 5). Further testing with the additional wavelength λ_{ex} 450 nm revealed consistent results,[22] and that SDr was both sensitive and specific for these AMD lesions.

Translational Application

The discovery of the sensitive and specific spectral signature SDr for drusen and drusen precursors, which can be detected in

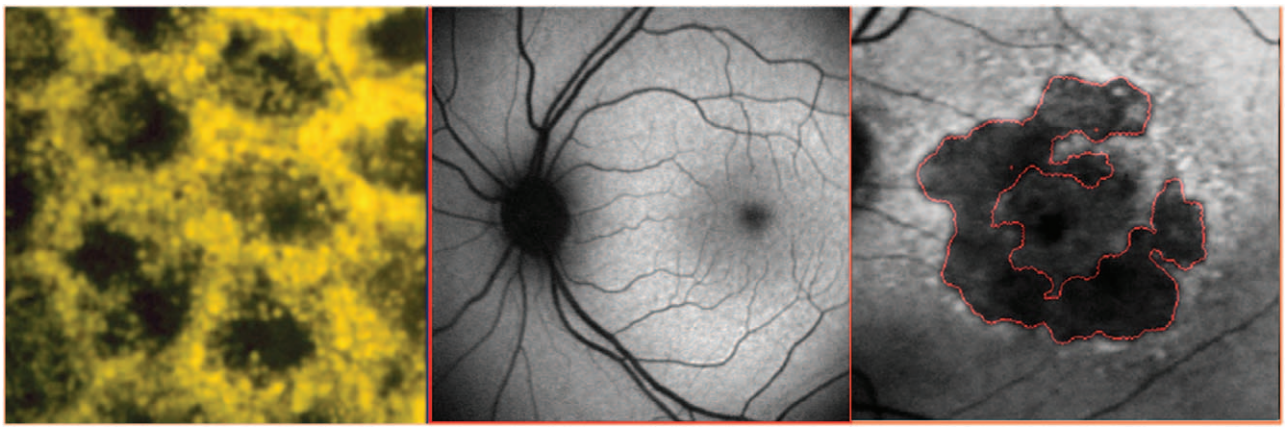

FIGURE 3. Left. Retinal pigment epithelium (RPE) bis-retinoids form complex granules known as lipofuscin, which increase with age, and glow gold under blue light. Middle. Normal gray scale FAF image. Right. fundus autofluorescence (FAF) image of subject with geographic atrophy (GA). The GA has a dark, but variable FAF, outlined in red.

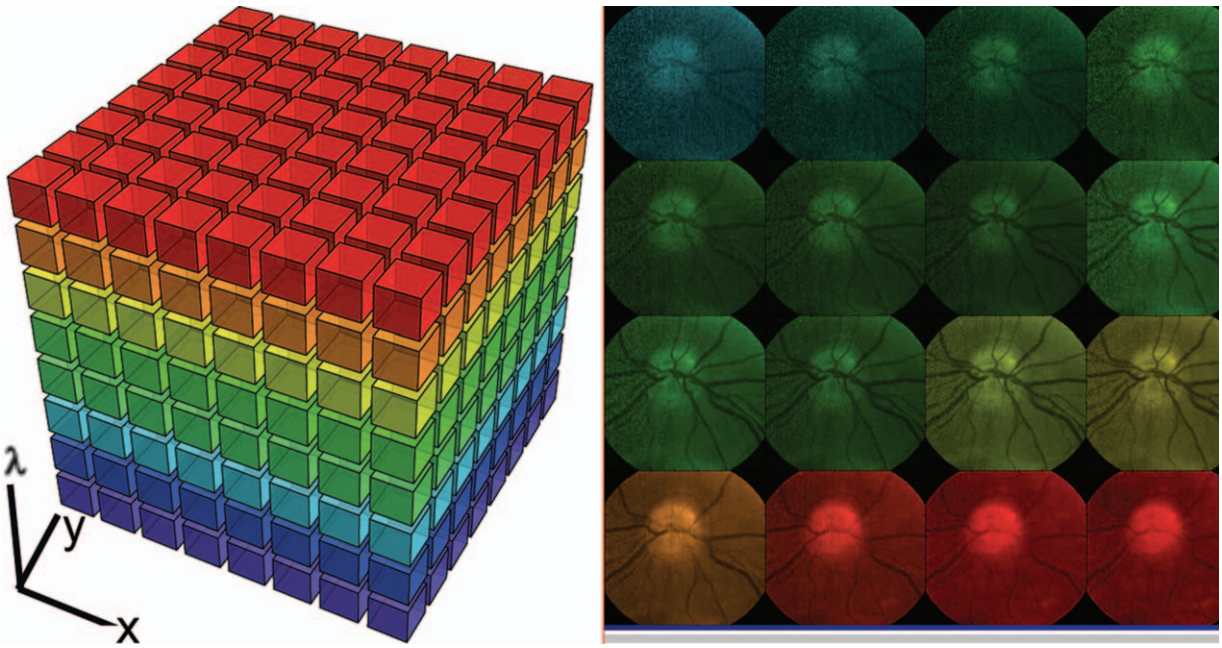

FIGURE 4. Left. Schematic of a hyperspectral data cube, wth 2 spatial dimensions *x*, *y*, and the spectral dimension λ. Right. Disc photo acquired in 16 wavelengths in the visible spectrum (ie, 16 colors). Each image can be considered one layer to be stacked into the corresponding hyperspectral image.

tissue with either blue or violet excitations 480 and 450 nm after mathematical separation from the usual AF emissions of the RPE, means that a clinical hyperspectral camera, with suitable image analysis, can be built for early detection of these signature lesions of AMD.

Such a camera is now being built in the laboratory of our collaborator Prof. Liang Gao at UCLA (NIH R01 EY029397) as part of a larger project with a dual function computational adaptive optics OCT for high-resolution structural imaging. To overcome the limitations of a cSLO, we will use instead the Image Mapping Spectrometer (IMS).[27] The IMS is a parallel acquisition instrument that captures a hyperspectral datacube without scanning. It also allows full light throughput across the whole spectral collection range due to its snapshot operating format. The IMS uses a custom-designed mirror, termed image mapper, which comprises multiple angled facets to redirect portions of an image to different regions on a detector array. A schematic is shown in Figure 6.

At the excitation side, we will filter the light source using a notch filter, illuminating the retina with 450 nm light. At the detection side, we will separate the RPE's AF from the reflected near-infrared light using a dichroic filter, each guided to a dedicated imaging channel. By registering the RPE's AF image with the correspondent OCT en-face image, we will be able to acquire both the functional and structural information of the retina within a single snapshot to detect drusen/drusen precursors for better staging and management of AMD.

TRANSLATIONAL TOPIC 3. THE OPHTHALMIC ENDOSCOPE FOR VITREOUS SURGERY

The ophthalmic endoscope is a major innovation for intra-ocular observation in vitreous surgery. An ophthalmic endoscopic system with technical specifications (FiberTech Co, Ltd, Tokyo, Japan) is shown in Figure 7. There are several advantages: fundus

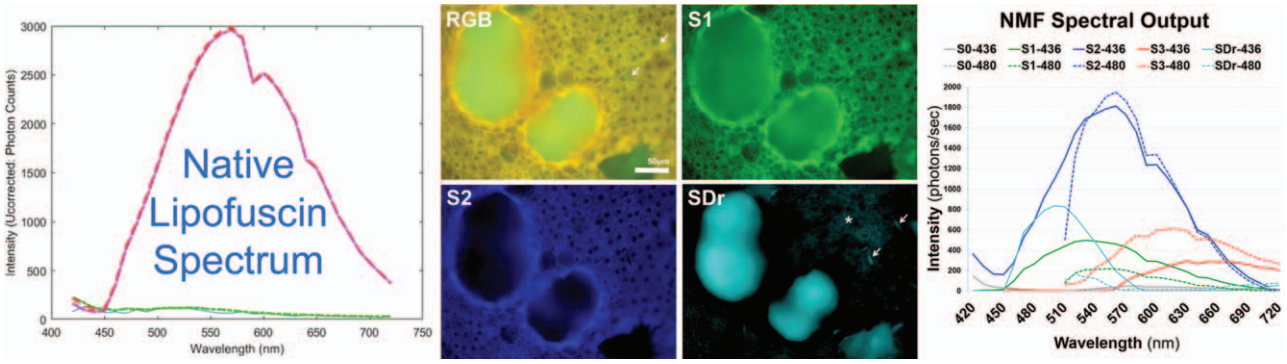

FIGURE 5. Left. The broad emission spectrum of RPE lipofuscin from a flatmount of RPE/BRM when excited by 436 nm light, captured by the Nuance camera. The peak in this sample is around 570 nm, in the yellow range (Compare Figure 1 Left). Middle and Right. The full color AF of the sample with drusen is marked RGB. Note again the predominantly yellow AF from the LF surrounding the nuclei in the RPE cells, whereas the AF from the soft drusen is greenish. Right. After mathematical ''unmixing'' of the AF from the sample, 3 distinct spectra are found in the RPE, labeled S1, S2, and S3, presented graphically in green, blue, and red, and a distinct new spectrum SDr (azure) is found that is specific for drusen/drusen precursors and has a short wavelength emission around 510 nm. Middle. The color-coded tissue localizations of the individual fluorophore sources of the spectra S1, S2 and SDr are shown (S3 not shown). AF indicates autofluorescence; BRM, bruch's membrane; RGB, composite red green blue autofluorescence image; LF, Lipofuscin; RPE, retinal pigment epithelium; SDr, spectrum for drusen.

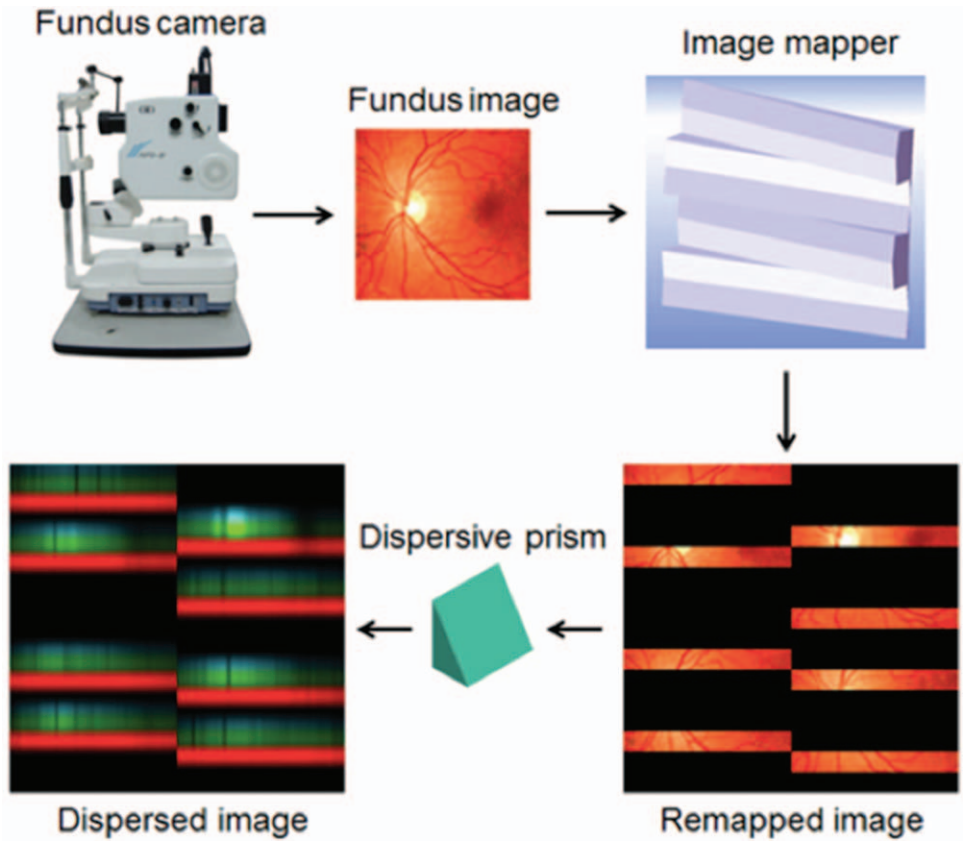

FIGURE 6. The IMS is a prism array that redirects slices of the image so that there is space between slices on the detector array. A prism or diffraction grating spectrally disperses the AF emission into all colors in the direction orthogonal to the length of the image slice. In this way, with a single frame acquisition from the camera, we obtain a spectrum from each spatial location (*x*, *y*) in the image, that is, a hyperspectral AF image. The spectral slices for each wavelength are then reconstructed into complete 2D images for each wavelength by a simple pixel remapping. This creates the final hyperspectral data cube for analysis by NMF. AF indicates autofluorescence; IMS, image mapping spectrometer; NMF, non-negative matrix factorization.

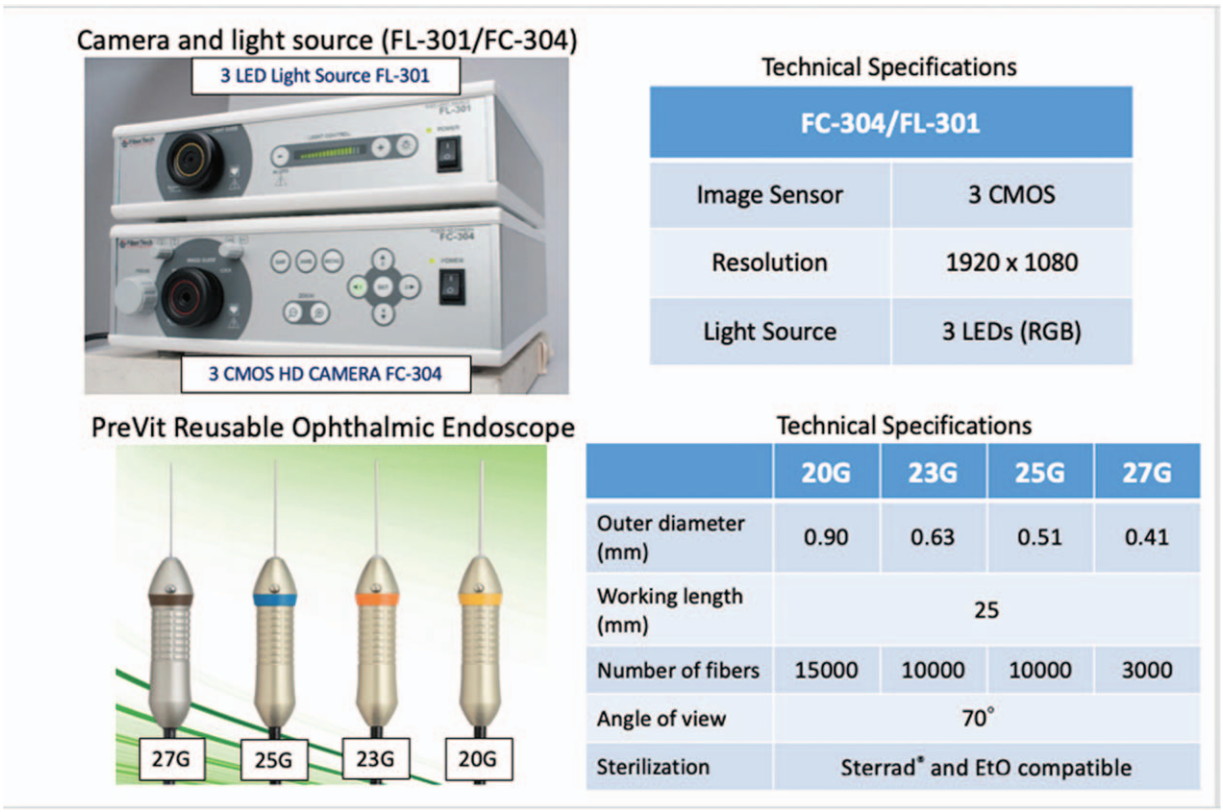

FIGURE 7. Ophthalmic endoscopic system (FiberTech, Tokyo, Japan). The resolution is of the image on the monitor. The actual tissue resolution is determined by the number of fibers in the scope and the proximity of the scope to the tissue (see Fig. 2A).

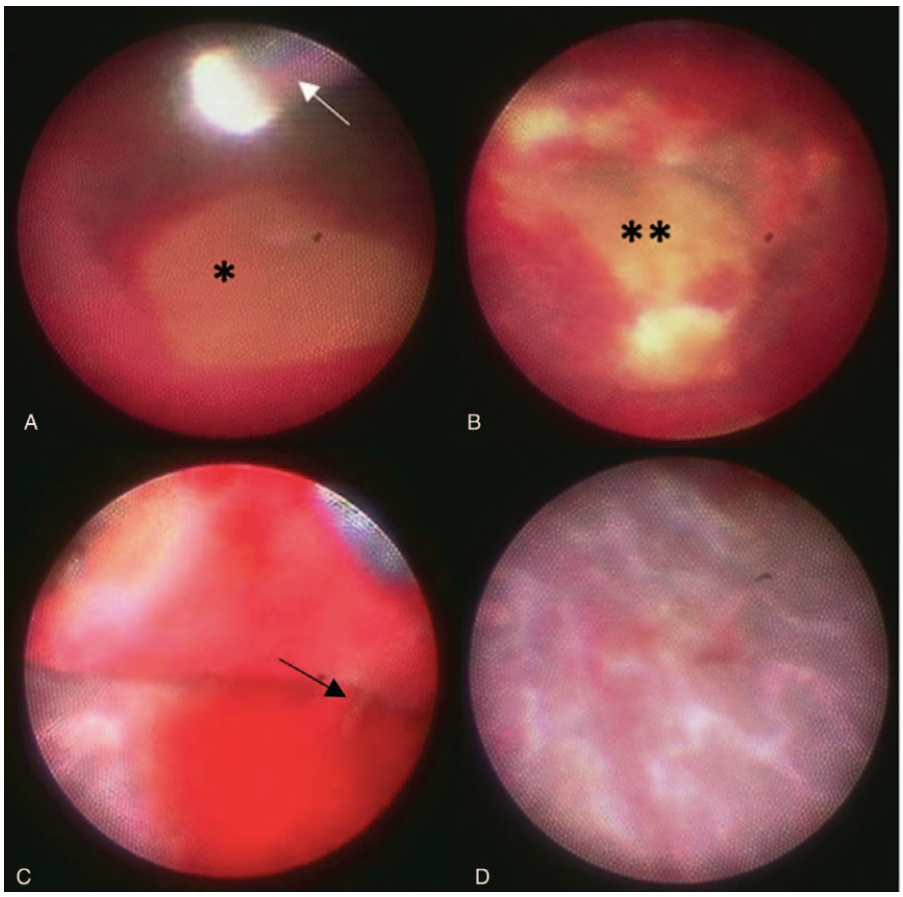

FIGURE 8. Ophthalmic endoscopic view (25G) under the retina in a PCV patient with a large subretinal hemorrhage (Modified from [33], with permission of the publisher). A, The retinal pigment epithelium (RPE) can be seen as an orange-colored tissue (asterisk) surrounded by remaining subretinal hemorrhage. The vitreous cutter is above (arrow). This entire field is about 2.5 mm in diameter, captured by the 10,000 fibers of the endoscope, giving about 20 microns per pixel resolution in this image. B, The CNV can be seen directly as a mass lesion of mosaic brown color (double asterisks). C, At the bottom of the CNV, a thin white cord-like tissue can be seen originating from the choroidal side, presumably a feeder vessel (arrow). D, After removal of the CNV, tortuous whitish choroidal vessels are observed, suggesting ischemia. CNV indicates choroidal neovascularization; PCV, polypoidal choroidal vasculopathy.

visualization is not impaired by opacities of the cornea or ocular media, pupil size or eye position. Furthermore, visibility of the entire fundus is stable during fluid-air exchange, with no areas hidden from view. Its usefulness has been demonstrated in complicated cases of ocular trauma, corneal opacities, small pupil, and endophthalmitis.[29–31] Ophthalmic endoscope-assisted vitrectomy is also useful in rhegmatogenous retinal detachment (RD) repair because it enables performance of subretinal fluid drainage through the primary retinal breaks by tilting the patient's head, and identification of small retinal breaks regardless of anterior segment conditions and air/gas exchange status.[32]

Kaga et al recently reported subretinal endoscopic surgery for removal of subretinal hemorrhage and choroidal neovascularization (CNV) completely without creating a large retinotomy in patients with a subretinal hemorrhage caused by neovascular age-AMD.[33] We begin this novel endoscopic vitreous surgery by injecting balanced salt solution and filtered air into the subretinal space to create a RD with a 38-gauge cannula (Extendable PolyTip, MedOne Surgical, Inc., Sarasota, FL,). We then position one trocar under the retina and switch the infusion from the vitreous to the subretinal space to maintain a large RD. Finally, we position another 2 trocars under the retina for insertion of the endoscope and vitreous surgical instruments for subretinal surgery under endoscopic guidance.[33]

Postoperative vascular endothelial growth factor (VEGF) inhibitors are not necessary in such cases because the CNV had been completely removed. Thus, this surgery, which has few postoperative complications, can be a good alternative for patients who are resistant to VEGF inhibitors or decline it for various reasons. In addition, it is possible to observe detailed subretinal findings at high magnification directly with the ophthalmic endoscope for better understanding of the disease process. Kaga et al reported direct observation of subretinal CNV, the RPE, choroidal vessels, and a presumed feeder vessel from the choroid to the CNV (Fig. 8). These endoscopic images of subretinal lesions, approaching high resolutions of 20 micron per pixel, are difficult to acquire by any other technique and we are convinced they are very valuable for understanding subretinal pathology. Image resolutions will be even greater in the future with higher numbers of fibers in the endoscope.

Translational Significance. Direct intraocular endoscopic visualization will be useful not only by enabling vitreoretinal surgical approaches heretofore impossible, but also by elucidating the pathogenesis of disease in conjunction with other imaging techniques.

TRANSLATIONAL TOPIC 4. REMOTE RETINAL IMAGING FOR TELEMEDICINE IN AMD AND DIABETIC RETINOPATHY

Retinal diseases such as AMD and diabetic retinopathy (DR) are on the rise due to increased longevity generally and increase of the diabetic population specifically. DR and AMD are the 2

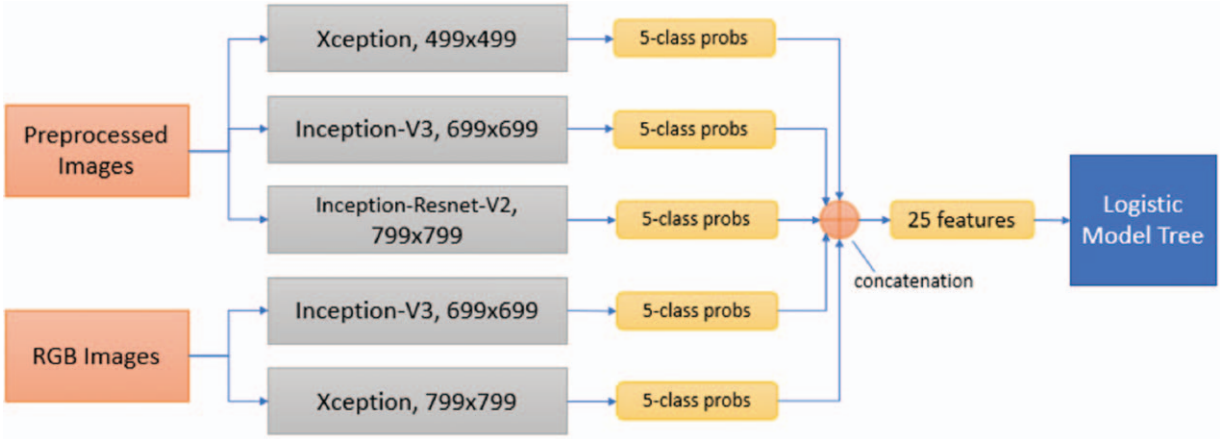

FIGURE 9. Ensemble framework of deep learning-based diabetic retinopathy (DR) screening system. The preprocessed and the original RGB images are input to ensembles of three and two deep learning models, respectively, differing in type of architecture and input image size. Each model then produces a set of 5 probabilities (probs) of belonging to each of the 5 DR classes: none, early, intermediate, severe, and PDR. The 25 total probabilities are then concatenated (grouped) to form a vector of 25 features which is input to a logistic model tree (LMT). The LMT has been trained to decide the DR class based on the totality of the deep learning inputs, and is the final classifier. PDR indicates proliferative diabetic retinopathy; RGB, red green blue images.

leading causes of blindness in the United States and other developed countries. Early detection is the key to prevention. However, screening for these disorders is generally done by eye specialists with limited availability to large segments of the population. Telemedicine solutions to this problem have been proposed to screen for AMD and DR with inexpensive nonmydriatic fundus cameras in primary care settings and automatic DL algorithms developed from big datasets. DL is a class of machine learning techniques that learns features directly from images without feature labels, and usually requires very large training datasets. In the recent years, DL has achieved breakthrough accuracy in image recognition tasks in different fields in ophthalmology like AMD, DR, and glaucoma.[34,35] The huge mass of retinal images generated by a high-volume telemedicine tool, which would overwhelm expert human graders, will require the efficiencies of DL for disease detection and stratification.

Our group has built DL architectures for screening DR and AMD. For DR, a DL system was built and validated prospectively.[36] Three DL neural networks were employed: Xception, Inception-V3 and Inception-Resnet-V2, each operating at 1 or 2 image resolutions to give 5 networks total and increase robustness to image features of different sizes. Each of the 5 networks then produces a set of 5 probabilities of a given image belonging to each of the 5 DR classes: none, early, intermediate, severe, and proliferative diabetic retinopathy (PDR). The 25 total probabilities are then input to a logistic model tree, combining logistic regression, and decision tree learning. The logistic model tree was trained to decide the DR class based on the totality of the DL inputs, and is the final classifier (Fig. 9). To test real world performance, we then examined prospectively acquired nonmydriatic retinal images from 974 diabetic patients in a primary care setting at the New York Eye and Ear Infirmary of Mount Sinai on a Topcon NW 400 camera between January 01, 2017, and December 31, 2017. A total of 814 patients were judged by 2 retina specialists to have no DR: 83 had mild DR, 12 had moderate DR, 2 had severe DR, and 5 had proliferative DR. These criterion standard gradings were compared with analysis of DL system, which achieved a sensitivity of 82.6% and a specificity of 93.7% for referral level DR.

For AMD, a DL system was built and validated prospectively on the age-related eye disease study (AREDS) dataset.[37] For AMD screening, we prospectively imaged both eyes of 160 unselected nondilated subjects older than 50 years at New York Eye and Ear faculty retina practices with a Food and Drug Administration-approved fundus camera (Eidon, Centervue Inc., Fremont, CA). After initial specialist review, 10 subjects with other confounding conditions like DR, myopia, vascular occlusion were excluded. One hundred eligible subjects (290 eyes, after further exclusion for image quality) were enrolled. All images were uploaded to the telemedicine platform and analyzed by a DL algorithm originally developed and tested on the AREDS datasets (Govindaiah et al, IEEE EMBC 2018:702–705) from iHealthScreen, an independent medical software company. To test the accuracy of the tool, the uploaded images were evaluated by 2 ophthalmologists and compared against the automated gradings by the software. Patients were classified as referable AMD (intermediate and late AMD) or nonreferable (normal macula and early AMD), based on the worst eye. After adjudication of human versus artificial intelligence (AI) discrepancies in grading (10 human and 7 AI errors), 66 subjects were referable and 84 were nonreferable AMD. For identification of early/none versus intermediate/late (ie, referral level) AMD, the tool achieved 88.67% accuracy with sensitivity of 86.57% and specificity of 90.36%.

The screening models using DL algorithms may prove to be public health assets through telemedicine. Creating a more comprehensive, fully effective system also trained on other retinal pathologies for public health service is both warranted and feasible. In conclusion, validated color fundus photo-based artificial intelligence platforms for DR and AMD screening are now ready for clinical testing, with potential for remote deployment and transformation of the very fabric of future medical care.

REFERENCES

1. Delori F, Greenberg JP, Woods RL, et al. Quantitative measurements of autofluorescence with the scanning laser ophthalmoscope. *Invest Ophthalmol Vis Sci*. 2011;52:9379–9390.

2. Gliem M, Muller PL, Finger RP, McGuinness MB, Holz FG, Charbel Issa P. Quantitative fundus autofluorescence in early and intermediate age-related macular degeneration. *JAMA Ophthalmol*. 2016;134:817–824.
3. Orellana-Rios J, Yokoyama S, Agee JM, et al. Quantitative fundus autofluorescence in non-neovascular age-related macular degeneration. *Ophthalmic Surg Lasers Imaging Retina*. 2018;49:S34–S42.
4. Spaide RF, Ooto S, Curcio CA. Subretinal drusenoid deposits AKA pseudodrusen. *Surv Ophthalmol*. 2018;63:782–815.
5. Smith RT, Sohrab MA, Busuioc M, Barile G. Reticular macular disease. *Am J Ophthalmol*. 2009;148:733–743.
6. Orellana-Rios J, Yokoyama S, Agee JM, Tong Y, Sakurada Y, Freund KB, Smith RT. Quantitative fundus autofluorescence of the junctional zone in geographic atrophy due to reticular macular disease (RMD). *Invest Ophthalmol Vis Sci*. 2018;59:3240.
7. Reiter GS, Told R, Schlanitz FG, et al. Impact of drusen volume on quantitative fundus autofluorescence in early and intermediate age-related macular degeneration. *Invest Ophthalmol Vis Sci*. 2019;60:1937–1942.
8. Reiter GS, Told R, Baratsits M, et al. Repeatability and reliability of quantitative fundus autofluorescence imaging in patients with early and intermediate age-related macular degeneration. *Acta Ophthalmol*. 2019;97:e526–e532.
9. Wang Y, Tran T, Firl K, et al. Quantitative fundus autofluorescence in smokers compared to non-smokers. *Exp Eye Res*. 2019;184:48–55.
10. Blacharski PA. Fundus flavimaculatus. In: Newsome DA, editor. Retinal Dystrophies and Degenerations. New York, NY: Raven Press; 1988: 135–159.
11. Allikmets R, Singh N, Sun H, et al. A photoreceptor cell-specific ATP-binding transporter gene (ABCR) is mutated in recessive Stargardt macular dystrophy [see comments]. *Nat Genet*. 1997;15:236–246.
12. Burke TR, Duncker T, Woods RL, et al. Quantitative fundus autofluorescence in recessive Stargardt disease. *Invest Ophthalmol Vis Sci*. 2014;55:2841–2852.
13. Sparrow JR, Gregory-Roberts E, Yamamoto K, et al. The bisretinoids of retinal pigment epithelium. *Prog Retin Eye Res*. 2012;31:121–135.
14. Duncker T, Lee W, Tsang SH, et al. Distinct characteristics of inferonasal fundus autofluorescence patterns in stargardt disease and retinitis pigmentosa. *Invest Ophthalmol Vis Sci*. 2013;54:6820–6826.
15. Duncker T, Tsang SH, Lee W, et al. Quantitative fundus autofluorescence distinguishes ABCA4-associated and non-ABCA4-associated bull's-eye maculopathy. *Ophthalmology*. 2015;122:345–355.
16. Duncker T, Tsang SH, Woods RL, et al. Quantitative fundus autofluorescence and optical coherence tomography in PRPH2/RDS- and ABCA4-associated disease exhibiting phenotypic overlap. *Invest Ophthalmol Vis Sci*. 2015;56:3159–3170.
17. Hood DC, Lazow MA, Locke KG, Greenstein VC, Birch DG. The transition zone between healthy and diseased retina in patients with retinitis pigmentosa. *Invest Ophthalmol Vis Sci*. 2011;52:101–108.
18. Schuerch K, Woods RL, Lee W, et al. Quantifying fundus autofluorescence in patients with retinitis pigmentosa. *Invest Ophthalmol Vis Sci*. 2017;58:1843–1855.
19. Duncker T, Greenberg JP, Ramachandran R, et al. Quantitative fundus autofluorescence and optical coherence tomography in Best vitelliform macular dystrophy. *Invest Ophthalmol Vis Sci*. 2014;55:1471–1482.
20. Gliem M, Muller PL, Birtel J, et al. Quantitative fundus autofluorescence in pseudoxanthoma elasticum. *Invest Ophthalmol Vis Sci*. 2017;58:6159–6165.
21. Smith RT, Post R, Johri A, et al. Simultaneous decomposition of multiple hyperspectral data sets: signal recovery of unknown fluorophores in the retinal pigment epithelium. *Biomed Opt Express*. 2014;5:4171–4185.
22. Mohammed T, Tong Y, Agee J, et al. Ex vivo hyperspectral autofluorescence imaging and localization of fluorophores in human eyes with age-related macular degeneration. *Vision*. 2018;2:38.
23. Fleckenstein M, Schmitz-Valckenberg S, Martens C, et al. Fundus autofluorescence and spectral-domain optical coherence tomography characteristics in a rapidly progressing form of geographic atrophy. *Invest Ophthalmol Vis Sci*. 2011;52:3761–3766.
24. Smith RT, Gomes NL, Barile G, Busuioc M, Lee N, Laine A. Lipofuscin and autofluorescence metrics in progressive STGD. *Invest Ophthalmol Vis Sci*. 2009;50:3907–3914.
25. Ben Ami T, Tong Y, Bhuiyan A, et al. Spatial and spectral characterization of human retinal pigment epithelium fluorophore families by ex vivo hyperspectral autofluorescence imaging. *Transl Vis Sci Technol*. 2016;5:5.
26. Tong Y, Ami TB, Hong S, et al. Hyperspectral autofluorescence imaging of drusen and retinal pigment epithelium in donor eyes with age-related macular degeneration. *Retina (Philadelphia Pa)*. 2016;36(suppl 1):S127–S136.
27. Gao L, Smith R T, Tkaczyk T S. Snapshot hyperspectral retinal camera with the image mapping spectrometer (IMS). *Biomed Opt Express*. 2012;3:48–54.
28. Ach T, Huisingh C, McGwin G, et al. Quantitative autofluorescence and cell density maps of the human retinal pigment epithelium. *Invest Ophthalmol Vis Sci Epub*. 2014;55:4832–4841.
29. Ren H, Jiang R, Xu G, et al. Endoscopy-assisted vitrectomy for treatment of severe endophthalmitis with retinal detachment. *Graefes Arch Clin Exp Ophthalmol*. 2013;251:1797–1800.
30. Sabti KA, Raizada S. Endoscope-assisted pars plana vitrectomy in severe ocular trauma. *Br J Ophthalmol*. 2012;96:1399–1403.
31. Yoshitake S, Oh H, Kita M. Endoscope-assisted vitrectomy for retinal detachment in an eye with microcornea. *Jpn J Ophthalmol*. 2012;56:613–616.
32. Yokoyama S, Kojima T, Mori T, et al. Clinical outcomes of endoscope-assisted vitrectomy for treatment of rhegmatogenous retinal detachment. *Clin Ophthalmol*. 2017;11:2003–2010.
33. Kaga T, Kojima T, Yokoyama S, Sato H, Yoshida N, Ichikawa K. Subretinal endoscopic surgery to treat large subretinal hemorrhages secondary to age-related macular degeneration. *Retina*. 2019;39:896–905.
34. Zapata MA, Royo-Fibla D, Font O, et al. Artificial intelligence to identify retinal fundus images, quality validation, laterality evaluation, macular degeneration, and suspected glaucoma. *Clin Ophthalmol*. 2020;14:419–429.
35. Gargeya R, Leng T. Automated identification of diabetic retinopathy using deep learning. *Ophthalmology*. 2017;124:962–969.
36. Bhuiyan A GA, Deobhakta A, et al. Development and validation of an automated diabetic retinopathy screening tool for primary care setting. Diabetes care. In Press.
37. Bhuiyan A WT, Shu D, et al. Artificial Intelligence to Stratify Severity of Age-related Macular Degeneration (AMD) and Predict Risk of Progression to Late AMD. *Transl Vis Sci Technol*. 2020:1960.